Rapid Communications

Linear and nonlinear coherent coupling in a Bell-Bloom magnetometer

R. Gartman,[1] V. Guarrera,[1,2,*] G. Bevilacqua,[3] and W. Chalupczak[1]
[1]*National Physical Laboratory, Hampton Road, Teddington TW11 0LW, United Kingdom*
[2]*Midlands Ultracold Atom Research Centre, School of Physics and Astronomy, University of Birmingham, Edgbaston, Birmingham B15 2TT, United Kingdom*
[3]*DIISM, Università di Siena, via Roma 56, 53100 Siena, Italy*

(Received 29 August 2018; published 13 December 2018)

Spin-exchange collisions in hot vapors are generally regarded as a decoherence mechanism. In contrast, we show that linear and nonlinear spin-exchange coupling can lead to the generation of atomic coherence in a Bell-Bloom magnetometer. In particular, we theoretically and experimentally demonstrate that nonlinear spin-exchange coupling, acting in an analogous way to a wave-mixing mechanism, can create additional modes of coherent excitation which inherit the magnetic properties of the natural Larmor coherence. The generated coherences further couple via linear spin-exchange interaction, leading to an increase of the natural coherence lifetime of the system. Notably, the measurements are performed in a low-density caesium vapor and for nonzero magnetic field, outside the standard conditions for collisional coherence transfer. The strategies discussed are important for the development of spin-exchange coupling into a resource for an improved measurement platform based on room-temperature alkali-metal vapors.

DOI: 10.1103/PhysRevA.98.061401

Introduction. Generating and maintaining coherence is essential for many precision measurement techniques based on atomic spin manipulation. Spin-exchange collisions (SEC) can be employed to transfer coherence between atoms of different species or in different states [1–10]. Coherence transfer has been demonstrated at high vapor densities and close-to-zero magnetic fields, in the so-called spin-exchange relaxation-free (SERF) regime, and at nonzero magnetic fields for atomic species with the same gyromagnetic ratios or following radio-frequency dressing of the atomic states. These schemes have been successfully implemented in a variety of different applications, including tests of fundamental physics [11] and cosmology [12], for quantum enhanced metrology [13], medical diagnostics [14], and navigation [15]. Recently, transfer of higher-order coherences has also been investigated and birefringence coherence has been shown to originate from the Larmor coherence within the same hyperfine ground state by a nonlinear spin-exchange collisional process [16]. Coherences of higher order than the Larmor are interesting as they are involved in phenomena such as the nonlinear magneto-optical rotation, which have been used for improved magnetometry schemes [17].

In this work, we experimentally demonstrate that the coherence oscillating at the Larmor frequency ω_{L} (natural coherence) can be effectively transferred to new *controllable* modes (secondary coherences). Magnetic properties of the former are transferred to the latter across different hyperfine states, notably in the regime of low atomic density and nonzero magnetic field. These conditions fall outside the standard regime for coherence transfer based on linear SEC coupling. We explain this effect as being due to the combination of the nonlinear coupling of the SEC term and the amplitude modulation of a relatively strong pump in a Bell-Bloom scheme ($\Omega_R \gg \omega_L$, with Ω_R being the Rabi frequency). We finally observe that the natural and secondary coherences can further interact in a linear fashion leading to 15%–25% narrowing of the Larmor coherence widths. This behavior reveals that modulation strategies might represent an important resource for manipulating coherences in optically pumped magnetometers, and that nontrivial resonance structures can appear even at low atomic densities when the pumping term is sufficiently strong.

Experimental system. We study the magneto-optical signal generated by a collective spin of Cs atoms in the $F = 3, 4$ ground states, precessing around a dc magnetic field. Measurements are performed in a low density (0.33×10^{11} cm^{-3}) thermal vapor housed in an antirelaxation, paraffin coated, glass cell. The atomic coherences are generated by a Bell-Bloom pumping process [18,19]. In this scheme a train of optical excitation pulses produces atomic coherences within both the ground-state manifolds (see Fig. 1). The $F = 3$ level is driven by resonant optical pumping and the $F = 4$ level is pumped mainly via SEC and optical off-resonance excitation [19]. We focus our analysis on the initial phase of the pumping process. As pointed out in [20] the spectrum of the evolving ground-state coherences contains, in that case, two components: (1) a steady-state oscillation at the modulation frequency ω_M and (2) a transient oscillating at ω_{L} damped on a time scale related to the SEC rate. In order to address them independently, the modulation of the pump is performed outside the standard frequency range of interest of a Bell-Bloom scheme, at a frequency ω_M whose integer multiples do not overlap with ω_L, i.e., $n \times \omega_M \neq \omega_{\mathrm{L}}$. In our setup, the atomic coherences are monitored by continuous Faraday-type polarization rotation measurements [21]. The polarization of

*v.guarrera@bham.ac.uk

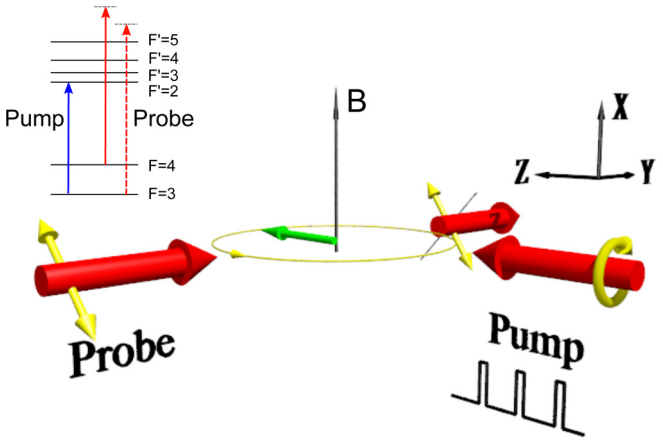

FIG. 1. Schematics of the experiment: a circularly polarized pump with periodically modulated amplitude creates a collective atomic spin (green arrow) orthogonal to the applied dc magnetic field (thin black arrow). The atomic spin precession is then probed by detecting the polarization rotation undergone by a linearly polarized off-resonant probe, propagating through the atomic sample orthogonally with respect to the pump beam and the applied magnetic field. The relevant transitions for pumping and probing on the ^{133}Cs D_2 line are shown.

the probe beam transmitted through the vapor cell is analyzed by a polarimeter. The magneto-optical rotation signal collected by a balanced photodetector is then analyzed to extract its Fourier transform, which, along with the continuous measurement, enables monitoring of the spectral components oscillating at frequencies other than the modulation ω_M. Details of our experimental setup can be found elsewhere [19]; we just recall here that the pump is obtained by a circularly polarized laser beam, frequency locked to the caesium $6\,^2S_{1/2}$ $F = 3 \rightarrow 6\,^2P_{3/2}F' = 2$ transition (D_2 line, 852 nm). The pump power is modulated with a square pulsed waveform and duty cycle of 7%. The signal produced by the $F = 4$ ($F = 3$) ground-state atomic coherences is read out by a probe beam propagating in a direction orthogonal to the pump beam, frequency locked to the $6\,^2S_{1/2}$ $F = 4 \rightarrow 6\,^2P_{3/2}F' = 5$ ($6\,^2S_{1/2}$ $F = 3 \rightarrow 6\,^2P_{1/2}F' = 4$) transition, and subsequently frequency shifted by 960 MHz to the blue side by two acousto-optic modulators in a double-pass configuration (see Fig. 1). The measurements are performed by scanning the frequency of the pump modulation across the value $\omega_0 = \frac{2}{3} \times \omega_L \simeq 2\pi \times 180$ Hz, which corresponds to the third harmonic of the square-shaped modulation coinciding with $2\,\omega_L$ [22].

Nonlinear coupling. The Fourier transform of the magneto-optical signal is shown in Figs. 2(a) and 2(b) for the $F = 3$ and $F = 4$ states, respectively. The peaks at $\omega_L \simeq 2\pi \times 270$ Hz corresponding to the transient oscillation are clearly visible, together with the first three harmonics of the square-shaped modulation function. Additionally, we observe several secondary peaks (and dips), appearing around the semi-integer multiples of the modulation frequency, whose positions shift as a function of ω_M and merge when $\omega_M = \omega_0$ according to the scaling $\omega_\pm = \frac{n}{2}\omega_M \pm \frac{1}{2}(3\omega_M - 2\omega_L)$, with n an odd integer. The signal shown in Figs. 2(a) and 2(b) was recorded during the first 4 s from the beginning of the optical pumping; however, we have verified that the contribution to the observed features comes solely from the transient dynamics, i.e., roughly the first 300 ms from the start of the pumping process when the induced natural coherences are present [23].

To better characterize the nature of the observed peaks, in Figs. 3(a) and 3(b) we report the position and linewidth of the secondary coherence profile moving across ω_L in $F = 4$ as a function of the modulation frequency [24]. We observe that its position (ω_{SC}) varies approximately linearly with the third harmonic of the optical excitation (fitted slope is 3.06 ± 0.02); in other words, the rate of change of its location follows the

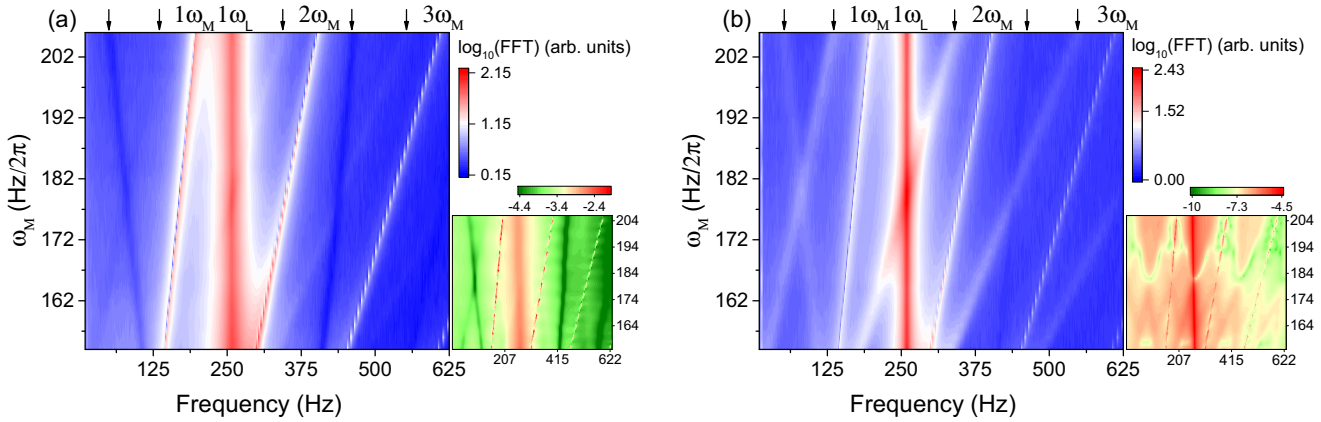

FIG. 2. FFT spectrum of the magneto-optical rotation signal detected for atoms in (a) $F = 3$ and (b) $F = 4$ for different frequency of modulation of the pump beam power. This portion of the spectrum shows the evolution around the Larmor frequency $\omega_L/2\pi \sim 270$ Hz. Together with the peak at ω_L and the first three harmonics of ω_M, additional peaks (and dips) depending on ω_M are visible around integer multiples of $\omega_M/2$ (highlighted by black arrows in the figure). The pump and probe beam powers have been set to 80 μW and 600 μW and for each modulation frequency the spectrum is the result of over 100 different acquisitions. Insets: calculated FFT spectrum of the average macroscopic spin component along the direction of the probe beam ($\hat{y}$ direction) for atoms in $F = 3$ and $F = 4$. The pump power has been set to $\Omega_R = 100\omega_M$, which corresponds to 20 μW power for our experimental settings. Due to computational issues we cannot simulate higher pump powers, for which we have compensated by using a stretched state to initiate the $F = 3$ ground state, mimicking saturation by a strong pump.

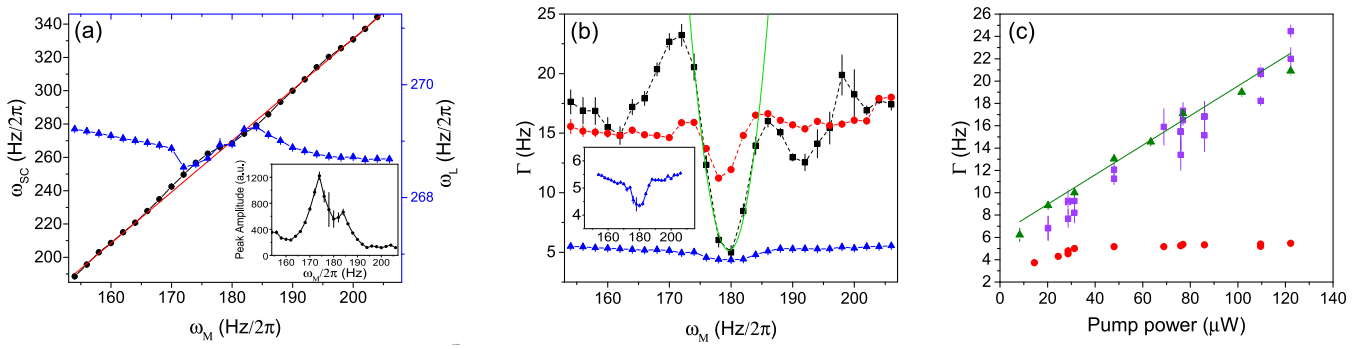

FIG. 3. (a) Positions of the FFT secondary coherence profile crossing ω_L (see text) as a function of the pump modulation frequency (black dots, scale on the left) and position of the natural coherence profile (blue triangles, scale on the right) for atoms in $F = 4$. The red solid line is a linear fit to the secondary coherence data providing the functional dependence $\omega_{SC} = (3.06 \pm 0.02)\omega_M - (272 \pm 2)$ Hz $\sim (3\omega_M - \omega_L)$. The inset shows the fitted amplitude of the secondary coherence profile as a function of the modulation frequency. (b) Linewidth of the natural coherence for atoms in $F = 4$ (blue triangles), secondary coherence for atoms in $F = 4$ (black squares), and Larmor coherence for atoms in $F = 3$ (red dots) as a function of the modulation frequency. The green solid line shows a quadratic fit to the secondary coherence data with function $\Gamma = (0.16 \pm 0.01)(3\omega_M - 2\omega_L)^2 + (5.1 \pm 0.4)$ Hz $\sim (\omega_{SC} - \omega_L)^2 + \Gamma_0$, where we have used the linear fit above for substituting ω_M. The inset of the figure is a zoom into the natural coherence linewidth for $F = 4$, showing a reduction of the peak size at resonance $\omega_M = \omega_0 = 180$ Hz. (c) Linewidth as a function of the pump beam power for the natural coherence of $F = 4$ atoms (red dots), the secondary coherence for $F = 4$ atoms (purple squares), and the natural coherence for $F = 3$ atoms (green triangles). For the secondary coherence profile in $F = 4$, measurements are taken on one side of the resonance with $160 < \omega_M < 170$ Hz. The green solid line is a linear fit to the $F = 3$ data. Each point in the above figures is obtained from the average of 100 acquisitions.

harmonic of the pump modulation around the birefringence coherence at $2\omega_L$. In addition, the linewidth Γ away from the resonance at $\omega_M = \omega_0$ for the atoms in $F = 4$ is compatible with the linewidth of the natural coherence profile measured for the atoms in $F = 3$. We recall that, because the pumping scheme implements direct optical excitation in the $F = 3$ and off-resonant transfer to the $F = 4$ level, the linewidths of the atomic coherences in these two ground-state levels differ significantly. This dependence is further confirmed by varying the power of the pump beam; see Fig. 3(c). Higher power broadening of the $F = 3$ coherence linewidth due to direct optical excitation can be seen in the linewidths of all the secondary peaks in $F = 4$. Transfer of characteristic features, such as the linewidth, from the $F = 3$ to the $F = 4$ level reveals transfer of coherences between the two different hyperfine states. Coherences in the alkali-metals' ground-state levels oscillate at opposite frequencies and there cannot be transfer due to linear SEC coupling between freely evolving modes. In the presence of a modulated pump, linear coherence transfer due to locking of the natural coherence to the external frequency drive has been demonstrated but only between different atomic species and the magnetic properties of one species, including its coherence time and gyromagnetic ratio, were not transferred to the other [8].

To provide intuitive insight into the nature of the SEC coherent coupling, we analytically solve the dynamics for a simplified system:

$$\frac{d\rho}{dt} = (W + Z + E)\rho + \epsilon Q(\rho)\rho + f(t)V, \qquad (1)$$

where the operators $W + Z + E = L$ denote the linear part of the Liouville equation [7], taking into account the hyperfine structure interaction $W\rho = A_{hfs}/(i\hbar)[\mathbf{I}\cdot\mathbf{S}, \rho]$, the external magnetic-field interaction $Z\rho = \omega_L/(i\hbar)[S_x, \rho]$, and the linear SEC interaction $E\rho = -R_{SE}(\mathbf{A}\cdot\mathbf{S})$. In the expressions above A_{hfs} is the strength of the hyperfine interaction, S_x is the component of the electronic spin along the direction of the magnetic field $\mathbf{B} = B\mathbf{x}$, and R_{SE} is the rate of SEC. The term due to the nonlinear SEC is $Q(\rho)\rho = R_{SE}(4\alpha\mathbf{S}\cdot\langle\mathbf{S}\rangle)$, which is weighed by an arbitrarily small amplitude ϵ in this perturbative approach. The operators α and $\mathbf{A}$ are the nuclear and electronic parts of the density matrix $\rho = \alpha + \mathbf{A}\cdot\mathbf{S}$. The simplest description for the amplitude modulated pump, allowing an analytical treatment, is obtained by introducing the additive term $f(t)V$, where $f(t) = \sum_n f_n e^{in\omega_M t}$, V is a diagonal matrix, and there is no direct dependence on ρ. We search solutions of Eq. (1) of the form $\rho(t) = \rho_0(t) + \epsilon\rho_1(t) + \cdots$ by solving the coupled equations:

$$\begin{aligned} \rho_0 &= L\rho_0 + f(t)V, \\ \rho_1 &= L\rho_1 + Q(\rho_0)\rho_1. \end{aligned} \qquad (2)$$

To derive the explicit expressions for the operators the density matrix is expanded as $\rho = \sum_{LM,FF'} \rho_{LM}(FF')|LMFF'\rangle$, by using the coupled spherical basis operators $|LMFF'\rangle$ [see Eq. (60) in [7]]. After simplifying the notation so that $\rho_{LM}(FF') = \rho_{\_i}$, one can find that $\rho_0\_i = A_i e^{\lambda_i t} + \sum_n w_{n,i} e^{in\omega_M t}$, while ρ_1_i is a sum of different modes with frequencies:

$$\begin{aligned} &\lambda_i \\ &\lambda_j + \lambda_k \quad \text{for } \lambda_j + \lambda_k - \lambda_i \neq 0, \\ &i(n+m)\omega_M \quad \text{for } -\lambda_i + i(n+m)\omega_M \neq 0, \\ &\lambda_j + in\omega_M \quad \text{for } \lambda_j - \lambda_i + im\omega_M \neq 0, \end{aligned} \qquad (3)$$

where the eigenvalues λ_i can be written as $\lambda_i = -\Gamma_i - i\,\omega_i$ [7,16]. The last term in Eq. (3) shows that the nonlinear SEC term in the presence of the pump modulation leads to the generation of secondary modes with frequencies depending on $(\omega_j + n\omega_M)$ and with magnetic properties inherited from the

natural coherences of the system Γ_j. In other words, nonlinear SEC induce a mode mixing of the magnetic multiplets and the stationary modes driven by the pump at the modulation frequency. This mode mixing, which cannot be found when only considering the linear part of Eq. (1), is compatible with what is observed in the experiment. To further confirm the results of our simple model, we have performed numerical simulations starting from the full master equation:

$$\frac{d\rho}{dt} = (W + Z + E)\rho + Q(\rho)\rho + \Lambda(t), \tag{4}$$

where the simple pumping term of Eq. (1) has been replaced by

$$\Lambda(t) = -L_R\{WW^\dagger, \rho\} + 2L_R W\rho_e W^\dagger + (\rho')_{sp}, \tag{5}$$

where $W = -E_0(t)\Pi\mathbf{d}\cdot\mathbf{e}^*\Pi_e$ [$W^\dagger = E_0(t)\Pi_e\mathbf{d}\cdot\mathbf{e}\Pi$], with $E_0(t)$ and $\mathbf{e}$ the amplitude and polarization versor of the laser field, respectively, and $\mathbf{d}$ the induced atomic dipole moment. Π and Π_e are the projectors on the ground and excited state (which is labeled with the letter e), and L_R is a coefficient depending on the natural linewidth of the transition. This term describes resonant pumping of the $F = 3$ level, while optical off-resonant pumping into the $F = 4$ level is neglected [25]. The first term in Eq. (5) accounts for depopulation of the ground state, while the second and third refer to repopulation due to stimulated and spontaneous emission. Using the expression obtained in [26], the latter term can be expanded into multiplets $\frac{d}{dt}\rho_{LM}(FF) = \sum_{F_e}\xi_L(F_e \to F)\rho_{LM}(F_eF_e)$ with

$$\begin{aligned}\xi_L(F_e \to F) &= (-1)^{F_e+F+L+1}(2J_e+1)(2F_e+1)(2F+1)\\ &\times \Gamma(J_e \to J)\begin{Bmatrix} F_e & F & 1\\ J & J_e & I\end{Bmatrix}^2\begin{Bmatrix} F & F & L\\ F_e & F_e & 1\end{Bmatrix},\end{aligned} \tag{6}$$

where $\Gamma(J_e \to J)$ is the natural linewidth of the transition and $\{\}$ is the Wigner 6-j symbol. We note that in the calculations we neglect the hyperfine coherences in the ground state and we include only the $L = 0, 1, 2$ terms in the expansion of the density matrix. The results of the numerical simulations, shown in the insets of Fig. 2, show good agreement with the main features of our experimental data. Additionally, they confirm that (1) the nonlinear coupling term is essential for explaining the secondary modes appearing in the spectrum and (2) the nonadditive terms in the pump of Eq. (5) are instrumental for recovering the precise frequency scaling which is experimentally observed. Concerning the latter point, we note that we can detect these secondary modes only for relatively strong pump power for which a simple description by an additive term is not appropriate anymore.

Linear coherence transfer. For linear SEC-driven coherence transfer it is essential that the coherences that are transferred in sequential random collisions are in phase. This imposes a resonance condition on the frequencies of the modes involved in the transfer, $\omega_{A,B}$, with respect to the time between the collisions τ_{SEC}, i.e., $(\omega_A - \omega_B) \times \tau_{SEC} < 1$ [4]. This condition is met when the spectral lines created by the atomic coherences, and coupled by SEC, overlap [9]. The range of detuning where coherence transfer can be observed is thus roughly defined by the SEC-limited width of the relevant spectral lines. As already discussed, the resonant condition is normally achieved in experiments by simultaneously adjusting $\omega_{A,B}$ with a magnetic field [6,7,9,10]. Characteristic signatures of coherence transfer are known to be (a) a reduction of the distance $(\omega_A - \omega_B)$ between the modes generated by coherence oscillation and (b) narrowing of the relevant profile linewidths following a quadratic dependence on the detuning $\Gamma \sim (\omega_A - \omega_B)^2$ [7]. In our case the strength of the coupling is not controlled by the magnetic field but by the modulation frequency of the pump amplitude. We focus our analysis on the secondary coherence profile ($\omega_A = \omega_{SC}$) moving across the natural coherence ($\omega_B = \omega_L$). In Figs. 3(a) and 3(b), signatures of the linear SEC coherence transfer can be observed. First, a detailed inspection of the change of the position of the secondary coherence peak (black dots) with ω_M reveals a deviation from the linear fit, shown with a solid red line in Fig. 3, well appreciable out of the measurement noise. This is mirrored by a change in the position of the natural coherence profile (blue triangles) within a ± 0.5 Hz range. Note that in the same interval of ω_M the secondary peak is also significantly amplified, as is clearly visible in Fig. 2 and in the inset of Fig. 3(a). Secondly, the secondary peak linewidth is significantly reduced and shows compatibility with a quadratic dependence on the detuning from the resonance $(\omega_{SC} - \omega_L)$, as shown in Fig. 3(b). On resonance, where the coupling is strong, the secondary coherence profile completely inherits the longer coherence time $T_2 = 1/\Gamma_B$ of the dominant natural coherence ($\Gamma_B \ll \Gamma_A$), which is mainly determined by SEC [10]. Notably, narrowing of the natural coherence profile linewidth by 15%–25% is also observed around the resonance for our experimental parameters. This suggests that the coupling of the natural and secondary coherence, which is a mixture of atomic multiplets of different hyperfine levels, counteracts the coherence relaxation due to SEC at the Larmor frequency, effectively increasing the associated coherence time T_2. This is similar to the linear SERF effect, as it follows a SEC-induced coherent hybridization of the quantum states of the atoms between the two hyperfine levels. However, unlike SERF we observe this effect in the unrestrictive regime of nonzero magnetic field and for rather low atomic density. Importantly this demonstrates that, in the case T_2 is limited by SEC, the controlled generation of hybrid coherences obtained in a *nonresonant* way can be used to induce SERF-like coherence improvement of Γ out of the typical SERF regime and enhance the operation of atomic magnetometers.

Conclusions. We have demonstrated that the magneto-optical signal of a Bell-Bloom magnetometer shows a rich spectrum dependent on the modulation frequency when a relatively strong pump is applied. This allows coherence transfer across different hyperfine states, a situation which cannot be achieved with linear SEC coupling in a regime of nonzero magnetic field and low atomic density, without further magnetic manipulation of the atomic states. We identify this effect as due to nonlinear coupling, as resulting from nonlinear SEC. The secondary coherences are thus created in a process that resembles a four-wave mixing scheme, led by collisional interactions between the atoms for our off-resonant pumping scheme—a situation previously observed only in momentum states of ultracold atoms [27]. The secondary coherences still linearly couple to the natural oscillation at ω_L, leading to

narrowing of the observed spectral profile and modification of its position. Our work shows that the combination of a controlled modulation and a nonlinear coupling term provides a rich scenario that can be exploited for improving spin coherence, and paves the way to new schemes for generating spin-squeezing in room-temperature vapor magnetometry [28].

Acknowledgments. The work was funded by the UK Department for Business, Innovation and Skills as part of the National Measurement System Programme. V.G. was supported by the EPSRC-UKRI (Grant No. EP/S000992/1). We thank G. Barontini, R. Godun, and R. Hendricks for critical reading of the manuscript.

[1] G. A. Ruff and T. R. Carver, Phys. Rev. Lett. **15**, 282 (1965).
[2] R. B. Partridge and G. W. Series, Proc. Phys. Soc. **88**, 983 (1966).
[3] G. W. Series, Proc. Phys. Soc. **90**, 1179 (1967).
[4] S. Haroche and C. Cohen-Tannoudji, Phys. Rev. Lett. **24**, 974 (1970).
[5] E. S. Ensberg and C. L. Morgan, Jr., Phys. Rev. A **3**, 2143 (1971).
[6] W. Happer and H. Tang, Phys. Rev. Lett. **31**, 273 (1973).
[7] W. Happer and A. C. Tam, Phys. Rev. A **16**, 1877 (1977).
[8] J. Skalla, G. Wäckerle, and M. Mehring, Opt. Commun. **127**, 31 (1996).
[9] W. Chalupczak, P. Josephs-Franks, B. Patton, and S. Pustelny, Phys. Rev. A **90**, 042509 (2014).
[10] O. Katz, O. Peleg, and O. Firstenberg, Phys. Rev. Lett. **115**, 113003 (2015).
[11] M. Smiciklas, J. M. Brown, L. W. Cheuk, S. J. Smullin, and M. V. Romalis, Phys. Rev. Lett. **107**, 171604 (2011).
[12] M. Pospelov, S. Pustelny, M. P. Ledbetter, D. F. Jackson Kimball, W. Gawlik, and D. Budker, Phys. Rev. Lett. **110**, 021803 (2013).
[13] W. Wasilewski, K. Jensen, H. Krauter, J. J. Renema, M. V. Balabas, and E. S. Polzik, Phys. Rev. Lett. **104**, 133601 (2010).
[14] X. Xia, A. Ben-Amar Baranga, D. Hoffman, and M. V. Romalis, Appl. Phys. Lett. **89**, 211104 (2006).
[15] T. W. Kornack, R. K. Ghosh, and M. V. Romalis, Phys. Rev. Lett. **95**, 230801 (2005).
[16] O. Katz, M. Dikopoltsev, O. Peleg, M. Shuker, J. Steinhauer, and N. Katz, Phys. Rev. Lett. **110**, 263004 (2013).
[17] S. Pustelny, W. Gawlik, S. M. Rochester, D. F. J. Kimball, V. V. Yashchuk, and D. Budker, Phys. Rev. A **74**, 063420 (2006).
[18] W. E. Bell and A. L. Bloom, Phys. Rev. Lett. **6**, 280 (1961).
[19] R. Gartman and W. Chalupczak, Phys. Rev. A **91**, 053419 (2015).
[20] Z. D. Grujic and A. Weis, Phys. Rev. A **88**, 012508 (2013).
[21] Y. Takahashi, K. Honda, N. Tanaka, K. Toyoda, K. Ishikawa, and T. Yabuzaki, Phys. Rev. A **60**, 4974 (1999).
[22] We note that the results obtained do not qualitatively depend on the chosen modulation frequency, provided the condition $n \times \omega_M \neq \omega_L$ is fulfilled.
[23] Observation of the weak stationary component at ω_L will be discussed elsewhere.
[24] Analogous components and similar behavior are observed in the $F = 3$ level.
[25] To clarify the role of off-resonant pumping to the $F = 4$ state in generating the observed peaks, we have repeated the measurements with the pump frequency red detuned with respect to the $F = 3 \rightarrow F' = 2$ transition by approximately 300 MHz (Doppler broadening is roughly 230 MHz). No qualitative difference was observed in the collected data, which justifies the predominance of SEC coupling between the $F = 4$ and $F = 3$ states.
[26] M. Ducloy and M. Dumont, J. Phys. **31**, 419 (1970).
[27] A. Perrin, H. Chang, V. Krachmalnicoff, M. Schellekens, D. Boiron, A. Aspect, and C. I. Westbrook, Phys. Rev. Lett. **99**, 150405 (2007).
[28] T. M. Hoang, M. Anquez, B. A. Robbins, X. Y. Yang, B. J. Land, C. D. Hamley, and M. S. Chapman, Nat. Commun. **7**, 11233 (2016).